
Article:
Mudenda, S and Kale, GM (2015) New insight into the electrical properties and ion dynamics of screen printed NASICON thick films. Journal of Materials Chemistry A, 3 (23). pp. 12268-12275. ISSN: 2050-7488

https://doi.org/10.1039/c5ta01660f

New insight into the electrical properties and ion dynamics of screen printed NASICON thick films

Steven Mudenda, Girish M. Kale*

Received Xth XXXXXXXXXX 20XX, Accepted Xth XXXXXXXXX 20XX
First published on the web Xth XXXXXXXXXX 200X
DOI: 10.1039/b000000x

Although AC conductivity measurements of NASICON is well documented in literature, thick film conductivity and ion dynamic studies, important for planar, are scarcely reported. Most thick film measurements are performed using four point probe methods (DC method) and are quite limited in that, they cant give information on ion dynamics and cannot seperate contributions from grains, grain boundaries and electrode effects. However, in this paper we report the electrical properties of NASICON, $x = 1.95$ thick films of different thicknesses (20-32 μm), screen printed on alumina substrates, in light of ionic dynamics using the AC conductivity formalism. Surface resistivities of thick films from impedance data in the frequency range $0.1 \leq f(HZ) \leq 3.2 \times 10^7$ is obtained. Impedance Cole-Cole plots shows grain interior and electrode effects. The hopping frequency and AC/DC conductivity are thermally activated and show Arrhenius-type behaviour, with activation energies in the range of $0.44 \leq E_a(eV) \leq 0.46$. Scaling in conductivity and Modulus shows that the relaxation mechanisms are independent of temperature and film thickness. Conductivity was independent of film thickness at high temperatures. SEM reveals that there is a minimum thickness for which NASICON on alumina substrate can be printed and used in high temperature planar electrochemical devices.

1 Introduction

NASICON is a well known family of fast sodium ion conductors, with a wide range of allowed stoichiometries, $Na_{1+x}Zr_2Si_xP_{3-x}O_{12}$ for $0 \leq x \leq 3$. Unlike sodium beta alumina (NBA) which conducts Na^+ ions in two dimensional plane, NASICON has 3D channels. This results in far better ionic conductivity than in NBA[1,2]. The conductivity is often high and is comparable to liquids at high temperatures[3]. The highest ionic conductivity is usually obtained for $x = 2$[2,4]. This is because at $x = 2$, the relative partial molar enthalpy of Na_2O is minimum and the relative partial molar entropy of Na_2O on the other hand is maximum, hence Na^+ ions are more mobile in this composition[5]. Because of this, NASICON finds extensive use in devices such as separation membranes, fuel cells and gas sensors[6–10].

In terms of thermal properties, NASICON shows low thermal expansion behaviours whose thermal expansion depends on the composition and the lowest value occuring at $x = 0.33$[11]. There is no information about crack formation in NASICON upon heating and cooling or due to thermal shock reported in the literature and the properties such as these has led to NASICON being used as solid electrolyte in planar gas sensors in form of thick films[3,6,8,10,12,13].

Ionic conductivities and related chacteristics are determined by using impedance measurements to avoid the need for non-blocking electrodes needed for DC measurements[14]. Using AC impedance measurements, conductivity as a function of frequency, hopping rates and ion dynamics of superionic materials can be obtained. This spectral analysis has been applied to Na-β"-alumina, $LiGaO_2$ and Ag/Na-mixed alkali β-alumina[15,16], NASICON type materials such as $NaNi_2ZrP_3O_{12}$, $Na_2(La,Co)TiP_3O_{12}$ and $Na_2(La,Al)TiP_3O_{12}$[14] and NASICON bulk material[17].

The need for miniaturising devices including sensors has seen the emergence of planar devices printed by screen printing technology for mass production[18,19]. For the fabrication of solid state gas sensors for example, NASICON is a suitable option as a solid electrolyte since it can be easily couple with commonly available auxiliary electrodes for indirectly sensing gases such as CO_2, NO_x, SO_x and H_2S that could not be otherwise realised using any other solid electrolytes. Just as it is well known that the bulk conductivity is greater than thick film conductivity[10], knowledge of the electrical properties of thick films to be used as electrolyte for planar sensors is vital. Although the conductivity measurements of bulk NASICON is well explored, the spectral studies are limited. In this paper, we report both the conductivity and spectral measurements of NASICON thick films from AC impedance measurements. The effect of film thickness on conductivity is also investigated. Also, the electrode configuration is in such a way that it resembles the configuration of commonly used planar NASICON based sensors[8,10,19] so that it can reflect real time electrical properties during sensing.

* *Tel: 0044-113-3432805 ; E-mail: g.m.kale@leeds.ac.uk*
Institute For Materials Research, University of Leeds, LS2 9JT, UK

Further in this paper, to isolate the intrinsic effects of thickness on conductivity from other phenomena that may influence surface conductivity, skin effect is investigated. Skin effect is the tendency of an alternating electric current (AC) to become distributed within a conductor such that the current density is largest near the surface of the conductor, and decreases exponentially with depths in the conductor[20]. The fact that this report also investigates the effect of film thickness on conductivity, it is important to establish also if NASICON thick films are prone to skin effect.

2 Experimental Methods

NASICON, $Na_{1+x}Zr_2Si_xP_{3-x}O_{12}$, of $x = 1.95$ composition was synthesized using the wet chemical route developed in our lab involving appropriate amounts of sodium citrate, zirconyl oxynitrate, TEOS and ammonium di hydrogen phosphate. The reaction medium was kept at pH of 2. The xerogel was calcined at 1000 °C to form NASICON phase. The powder was then ground and milled overnight to break agglomerates.

To make the slurry, ethyl cellulose (EtC), furoic acid (FA), butyl carbitol acetate (BCA) were used, with acetone as a diluting agent. This recipe was developed by Wang and Kumar[10]. The solid loading of NASICON was 55.8% while the rest has a mass ratio of 1 : 0.058 : 0.12 corresponding to BCA, FA and EtC repectively.

An Aurel MOD C380 screen printer was used for screen printing. To vary the thickness of NASICON film on the alumina substrate, different printing cycles were used where the least number of printing strokes represent the thinnest layer. The screen stage was also raised after each cycle to accomodate the new additional layers. Three substrates were printed, the first sample printed with only one double stroke (DS) cycle denoted as 1DS , the second, with two cycles (2DS) and the third with three cycles (3DS) respectively. A double stroke (DS) is the printing where the squegee prints in both forward and backward direction. After printing, the NASICON thick film samples were left for 10 minutes in air to level up until they were smooth. They were then dried at 70 °C to firmly fix the thick film onto the substrate. The samples were then sintered in a tube furnace at different temperatures and sintering times to obtain the best sintering conditions. A sintering temperature of 1100 °C for 60 minutes yielded a well sintered film with only traces of zirconia. A cross section of each film was investigated under SEM to determine film thickness and phase composition. The thicknesses of samples 1DS, 2DS and 3DS were found to be 20 μm, 31 μm and 32 μm respectively. This was determined by SEM. Figure 1 shows the schematic of the printed NASICON and the Pt contacts with respect to the film.

The platinum ink was then printed on top of the film, by printing two parallel strips of conductive Pt ink. It was then then dried at 70 °C after which it was fired at 850 °C for 30 minutes to platinize the film. Finally Pt wire was connected onto the printed Pt strips and held in place with Pt paste. It was dried and then fired for 30 minutes at 850 °C. The AC measurements were performed using the Solartron 1260, while the rig was housed in the Faraday cage within a horizontal tube furnace.

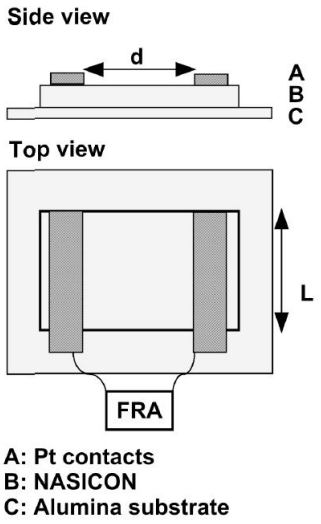

Fig. 1 Schematic showing the geometry of screen printed NASICON thick film on alumina substrate and the Pt contacts.

3 Results and Discussions

3.1 XRD

To ascertain that the NASICON phase is well preserved after sintering, XRD was performed on the sintered films. There is a narrow window between the sintering temperature and sintering time for which a well densified and zirconia free NASICON film can be obtained. It was found that if the film is sintered at $T < 1100$ °C for less than 60 minutes the film would not be well sintered and this would negatively affect film conductivity. On the other hand if the sample is sintered for over 60 minutes, or at temperatures, $T > 1100$ °C, the film would be well sintered and become glassy all at the expense of phase quality. Rapid loss of Na_2O and P_2O_5 due to volatilization degrades the NASICON phase leading to mixture of NASICON and zirconia as has been reported elsewhere[21,22]. Zirconia reduces the conductivity as it is insulative[23]. A compromise between NASICON purity and densification had to be reached. Therefore an optimum sintering temperature at $T = 1100$ °C for 60 minutes has been selected. Figure 2 shows the XRD reflections of the three NASICON thick films.

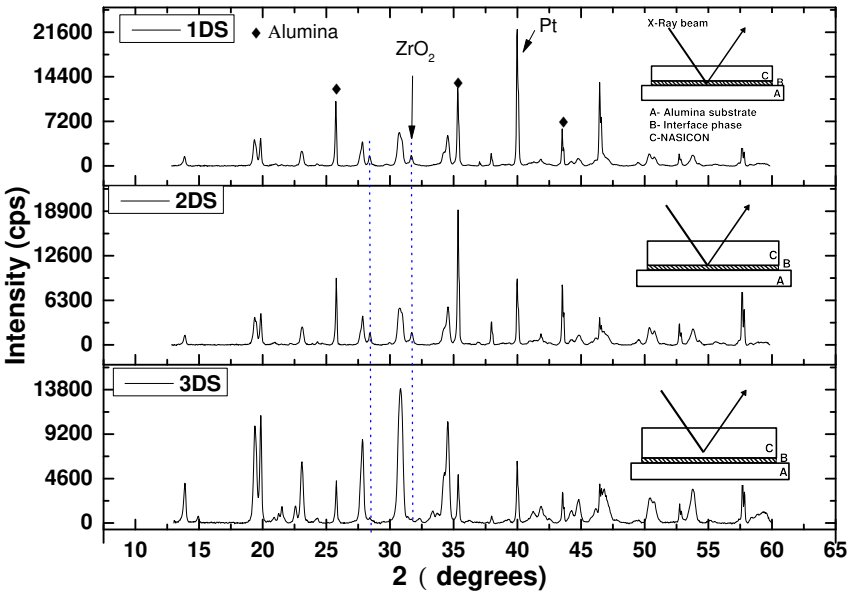

Fig. 2 XRD reflections for the thick film NASICON sintered at 1100 °C for 60 minutes. The insets are a sketch of the proposed reason why a zirconia phase is observed in thinner films, 1DS, 2DS and not in the thicker film, 3DS.

The thinner films, 1DS and 2DS had some observed traces of zirconia. Possible reasons for the observed zirconia are (1) loss of Na_2O and P_2O_5 through volatilization and (2) reaction of Na_2O and Al_2O_3 at the interface of NASICON with alumina substrate leading to zirconia precipitates. The fact that the thicker film, 3DS, does not show the zirconia phase implies that the presence of zirconia in 1DS and 2DS thick films is not to a large extent due to the volatilization as reported by other workers but due to this very interfacial reaction of of Na_2O and Al_2O_3. The compositional change infact occured at the interface of NASICON and the alumina substrate. This is discussed in more detail in section 3.2 of SEM measurements. On the other hand, in terms of densification, the thinner films were more smooth and shinny showing better densification and this positively impacted on the electrical conductivity.

3.2 SEM

Figure 3 shows a backscattered image of a cross-section of NASICON thick film sample after AC impedance measurements. It can be seen that NASICON underwent a compositional change at the interface that was in contact with the alumina substrate. EDX mapping, not shown here, showed that the interface is Na deficient, and believed to be composed of ZrO_2 with traces of dissolved Na or sodium zirconate Na_2ZrO_3. There was also a small trace of aluminium noticed the NASICON matrix.
The thickness of the interface layer was found to be constant in all the samples, that is, it was indepedent of the NASICON film thickness. It was found to be approximately $7 \pm 1\ \mu$m.

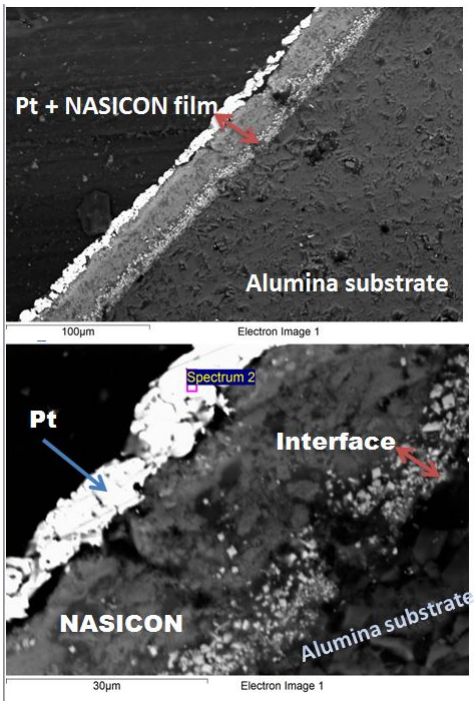

Fig. 3 Backscattered SEM image of NASICON thick film (2DS) on alumina substrate coated with Pt and fired at 1100 °C for 60 min. A zirconia rich phase is observed at the interface.

This implies that there is a minimum thickness of NASICON that can be printed and used in high temperature applications, that is $\geq 7\ \mu$m in order to retain the original intrinsic properties of NASICON. From the XRD patterns and the inset sketches in Figure 2, since the thickness of the interface layer is constant, X-rays were able to penetrate through the entire thickness of NASICON film up to the interface except in the thickest film, 3DS examined in this study. This could have been the probable reason for observing zirconia traces in the thinner films and not in the thickest film, 3DS in XRD patterns shown in Figure 2 of Section 3.1. In terms of electrical conductivity therefore, the presence of zirconia at the interface would not seem to affect the surface ionic conductivity unless the film is less than 7 ± 1 μm thick.

3.3 Electrical Characterisation

The measurements obtained here are related to the surface conductivity measurements. There is limited or no information in the literature on the AC impedance measurements of NASICON thick film with the present electrode configuration. Based on the sample dimensions and electrode configuration shown in Figure 1, the surface resistivity (ρ_s) is determined from surface resistance (R_s). R_s or $Z_s(\omega)$ is the ratio of voltage V to the current I_s flowing between the two electrodes. Thus

$$R_s = \frac{V}{I_s} = Z_s(\omega) \tag{1}$$

Surface resistivity, (ρ_s) on the other hand is the ratio of voltage drop per unit length d to the surface current I_s per unit length L[24,25]. Using this ratio and Equation (1) we obtain

$$\rho_s = \frac{V/d}{I_s/L} = \frac{V}{I_s} \cdot \frac{L}{d} = Z_s \cdot \frac{L}{d} \tag{2}$$

The units are ohm/square (Ω/sq). From the measured impedance, conductivity is deduced using the reciprocal of Equation (2).

Normally when a sample is connected to the AC impedance analyser, it is connected with wires. Therefore the overall impedance is a sum of complex impedance contribution from the wires ($Z_{wire}(\omega) = R + i\omega L$), sample electrode interface $(Z_{SEI}(\omega))$ and complex impedance from the sample$(Z_{sample}(\omega))$ so that $Z = Z_{sample}(\omega)$ + $Z_{wire}(\omega)$ +$Z_{SEI}(\omega)$ where R and L are the resistance and inductance of the wire respectively. Complex impedance measurement is able to resolve these processes so that the true electrical properties of the sample can be obtained.

3.3.1 AC Conductivity. Figure 4 is a Cole-Cole plot of 1DS NASICON thick film at different temperatures shown in the legend. Only single semi-circles can be observed representing a contribution from only grain interiors $(Z_{sample}(\omega))$ suggesting a single relaxation process. There is also a low frequency tail that corresponds to sample electrode interface $(Z_{SEI}(\omega))$. It can be seen that ionic conductivity is temperature activated and that the existence of these perfect semi circles implies that not only does ions conduct in bulk materials but on the surfaces too.

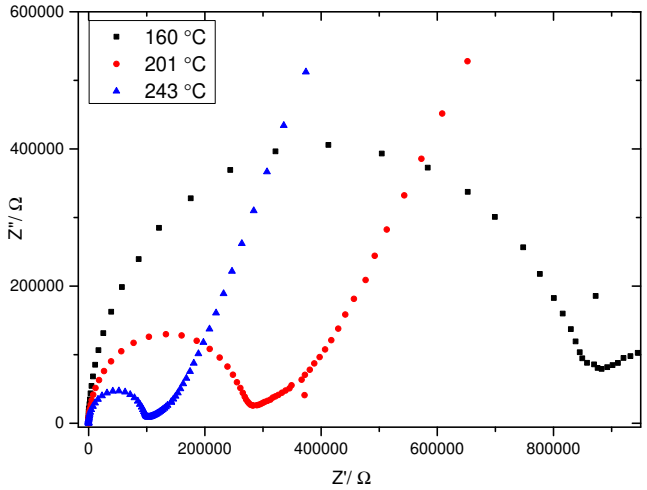

Fig. 4 Cole-Cole plots obtained from the impedance measurements of the 1DS sample, from frequency range of 32 MHz to 0.1 Hz. Only single semi-circles are evident corresponding to grain interior.

In a thermally activated process, the temperature dependence of conductivity is represented by the Arrhenius relation in eqn (3);

$$\sigma T = \sigma_0(T) \exp\left(-\frac{E_a}{kT}\right) \tag{3}$$

where $\sigma_0(T)$ is a pre-exponetial factor which is a function of charge carrier concentration, temperature and material structural parameters, k is the Boltzmann constant and E_a is the activation energy of conduction.

Figure 5 is the Arrhenius plot which indeed follows the relationship in eqn (3). The plots show a signature of a temperature activated process. Comparison of conductivity with temperature in Figure 5a shows that conductivity is independent of film thickness at higher temperature. Despite the fact that Arrhenius plots for bulk NASICON usually exhibit two linear segment plots representing two activation energies, the plots in Figure 5 for thick films hardly bring out the two segments with an exception of the thicker film (3DS). Figure 5b for the thinnest film (1DS) only show a small deviation at $T = T_{trans} \simeq 201$°C, a temperature believed to be the transition temperature from a monoclinic to rhombohedral crystal structure of NASICON. A first derivative of plot resolves the transition temperature as is shown in the inset of Figure 5b.

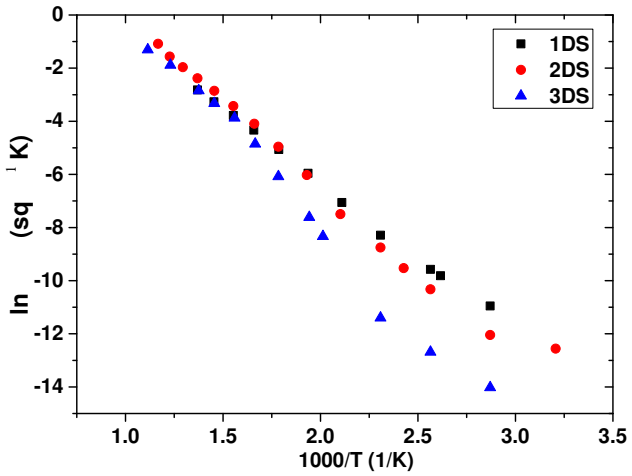

(a) Arrhenius plots for films of the different thicknesses. Above 300 °C the conductivity is independent of film thickness

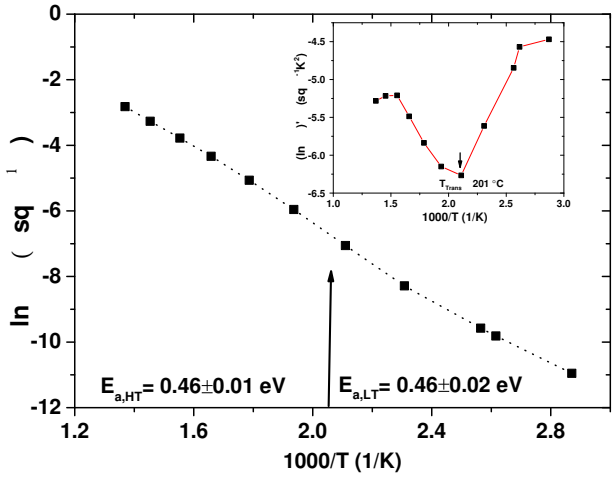

(b) Arrhenius plot for the single double stroke(1DS). The inset is a first derivative of $ln\sigma T$ w.r.t 1000/T

Fig. 5 Arrhenius plots for the NASICON thick films.

The activation energies on either side of T_{trans} for low temperature (LT) and high temperature (HT) regions is $E_a =$ 0.46 eV. This value is higher than reported in literature for bulk NASICON but better than 0.57 eV obtained by Wang and Kumar [10] on alumina containing NASICON film and close to the value reported by Funke [15], Fuentes *et al.* [26,27] on pellets. From this finding it is apparent that the ions encounter a higher energy barrier in surface conduction than in bulk. Possible reasons being the precipitation of a resistive zirconia phase due to the partial volatilization of sodium and phosphorous oxides on the surface of the films [23] and also from the interfacial reaction between alumina and NASICON. Further, apart from the zirconia which precipitated at the interface, there were also some traces of aluminium diffused into the NASICON matrix which probably impeded ionic conductivity.

Comparison of conductivity as a function of temperature also reveals that there is no systematic dependence of conductivity with thickness above 600 K indicating that conduction is indeed a surface phenomenon in NASICON thick films.

3.3.2 Skin Effect.

To ascertain if the independence of surface conductivity with film thickness especially at higher temperatures is due to skin effect, the skin depth (δ_s) was calculated as a function of frequency and conductivity. This is given by $\delta_s = \sqrt{\frac{2}{\sigma\omega\mu}}$, where σ is the material conductivity, $\mu = \mu_r\mu_o = 4\pi \times 10^{-7}$ H/m is the conductivity magnetic permeability and ω is the radian frequency [20]. The value of μ_r is taken as unity for a non magnetic material such as NASICON. This implies that the electrical conduction will only be limited to the skin of the surface regardless of the thickness thereby masking the intrinsic effects of thickness or interfacial reaction between substrate material and NASICON, on surface conductivity. A plot of skin depth vs frequency at each temperature is given in Figure 6. It can be seen that due to lower magnitude of the surface conductivitites in NASICON, skin effect does not have significant influence on the overall conductivity of NASICON in the experimental condition as the calculated values of skin depth are, $\delta_s \gg t$ where t is the film thickness. The insert of Figure 6 is skin depth as a function of temperature at a frequency of 32 MHz, representing the smallest skin depth at each temperature in the present experimental setup. The smallest skin depth is $\sim$ 9.85 m and occured at a temperature of 457 °C indicating immunity of thick film NASICON to skin effect.

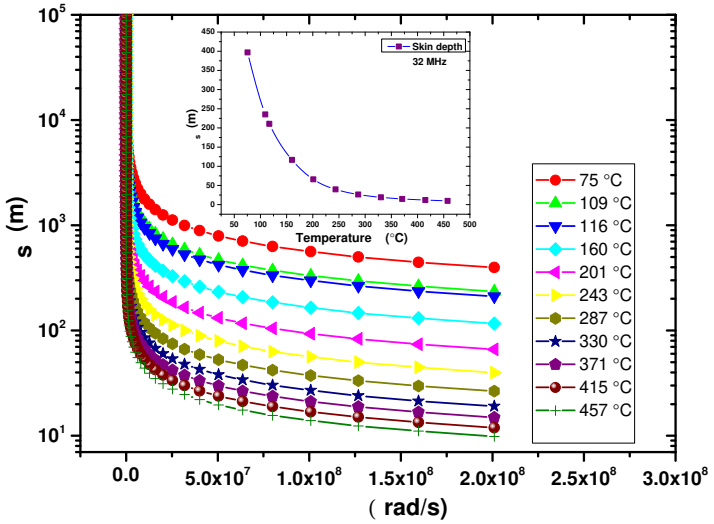

Fig. 6 Skin depth as a function of radian frequency. The inset is a plot of skin depth as a function of temperature.

3.3.3 Spectral Analysis. Measurement of AC conductivity generally shows a frequency dispersion where, the real part of AC conductivity ($\sigma'(\omega)$) is frequency (ω) dependent. Each curve may be characterized by a low-frequency plateau, which corresponds to the DC conductivity of the material, and a dispersive region at high frequency, which corresponds to the ionic or AC conductivity. The behavior obeys the Jonscher's power law[28] and it is found to vary with angular frequency according to eqn (4);

$$\sigma = \sigma_{DC} + A\omega^n \tag{4}$$

where σ_{DC} is the DC conductivity, A and n are temperature-dependant parameters.

Frequency dependence of conductivity of the thinnest sample (1DS) of NASICON examined in this study at various temperatures is shown in Figure 7. Three regions are observed here. Low frequency dispersive region, plateau and high frequency dispersive region. The first low frequency dispersive region may be due to polarization effects (sample electrode interface phenomena (SEI)). This is because as frequency decreases, more and more charge accumulation takes place at the interface leading to a decrease in the number of mobile ions subsequently lowering the conductivity. This was also observed by other workers[29,30]. Furthemore, the relaxation time could be as long as 10s hence giving enough time for ion polarization to take place. Since electrode effect is more pronounced at high temperatures this could be the reason for the spectra are curving in to almost zero in higher temperature plots of Figure 7. The plateau represents the DC conductivity and is independent of frequency. The second dispersive region at high frequency ($(10^4 - 10^8)$Hz) represents the AC ion conductivity. In this region the mobility is high hence conductivity increases with increasing frequency. This second dispersive-plateau pair is the distinct nature of non-random hopping mechanism.

In Figure 7, it can be clearly seen that the crossover frequencies ω_p increases with temperature or shifts towards high frequency with increase in temperature. The crossover frequency is a frequency at which transition from DC conductivity to AC dispersion occurs. The logarithmic plot between DC conductivity and cross over frequency (ω_p) shown as a solid line in the plot of Figure 7 inset gives a unity slope, which perfectly agrees with the AC conductivity formalism[15] implying that the DC and AC conductions are closely correlated to each other and that they are of the same mechanism[31] or that the characteristic angular frequency ω_p is activated with same thermal activation energy as the dc conductivity[30,32].

Non-linear fitting (with a goodness of fit ≥ 0.98) of data in Figure 7 using Equation (4) the dispersion-plateau pair gave $n < 1$ implying that the hopping motion of Na^+ in NASICON is a big hop translational motion.

Comparison of DC conductivity obtained from the low frequency plateau with AC conductivity using the Arrhenius

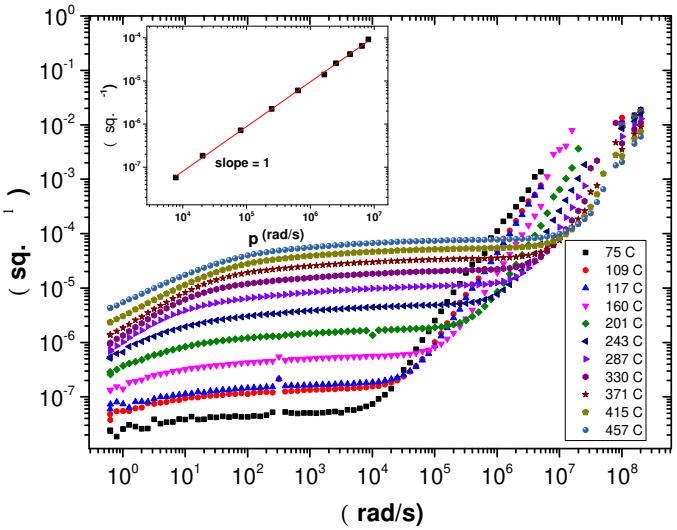

Fig. 7 Conductivity dispersion of NASICON for the 1DS sample. Two dispersions and plateaus are observed indicating a multiple activation energies. The inset is a plot of log σ vs log ω_p.

relation is shown in Figure 8. The close correlation in the values implies that the conduction is from the same majority charge carrier, the Na^+, in this case. This also suggests a high transference number of Na^+ in NASICON.

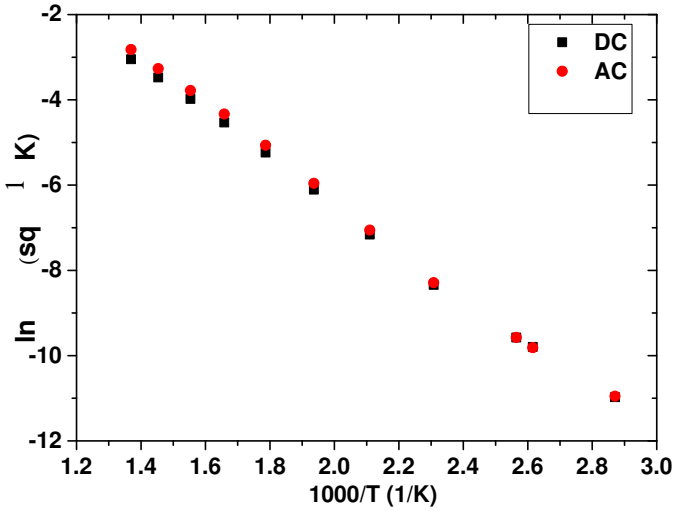

Fig. 8 Comparison of DC conductivity obtained from the low frequency plateau with AC conductivity.

To study the dynamics of relaxing species, electric modulus formalism is employed. Electric complex modulus is related to complex impedance by[33]

$$M^* = j\omega C_o Z^* = M' + jM''. \tag{5}$$

so that substituting $Z^* = Z' - jZ''$ into eqn (5) yields $M'' = \omega C_0 Z'$, where C_0 is the vacuum capacitance from the two parallel electrodes. For two parallel plates of area A and separation L, $C_0 = \varepsilon_0 \frac{A}{L}$.

The exact values of M'' in this report were not determined owing to the complex nature of the vacuum capacitance C_0 between the two electrodes of the sample configuration in thick films shown Figure 1. This is because the electrodes that are in contact with the NASICON are not parallel plates anymore but can be modelled as two parallel wires of capacitance, $C_0 = \frac{\pi\varepsilon_0}{ln(d/a)}$, where a is the radius of each electrode wire and this is difficult to determine in the current setting [34]. However, since M'' is dependent of Z' and ω, the relaxation processes and ion dynamics can be studied without the need to know the constant C_0. Therefore the plot of M''/C_0 vs frequency will still reserve the shapes of the peaks to yield the much needed data of crossover frequencies.

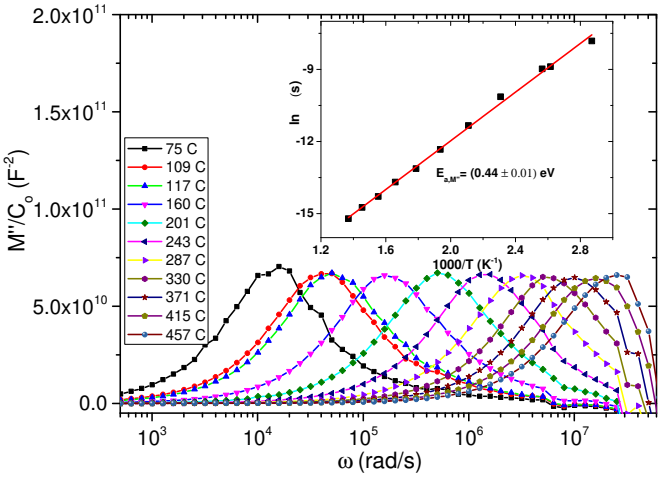

Fig. 9 Electric Modulus of NASICON thick film (1DS). Peak frequency decreases with temperature showing a thermal activated process. The inset is the Arrhenius plot of relaxation times.

In Figure 9 the variations of imaginary component of (M''/C_0) as a function of frequency (ω) at different temperatures show clearly resolved peaks at unique peak frequencies, with the peaks showing a tendency to shift towards higher frequency end with increase in temperature. This behaviour suggests a conduction mechanism which is a thermally activated type of correlated hopping of Na^+ ions. The crossover frequency (ω_p) is the frequency of transition from long range to short range hopping of ions from the low frequency to high frequency regions respectively. The high frequency side of M''/C_0' represents the range of frequencies in which charge cariers can only make localized motions within their spartial confinement of potential wells [29,35]. The inverse of the crossover frequency gives the characteristic relaxation time and follows the relation $\tau_M = \tau_{o,M} \exp(E_{a,M}/kT)$ where τ_o is a pre-exponential factor of relaxation time and T is the absolute temperature. This relation is shown in the inset of Figure 9. The activation energy of relaxation is $E_{a,M} = 0.44 \pm 0.01$ eV which is comparable with the conduction activation energy value of 0.46 eV obtained in this study. This result implies that ions have to overcome same energy barrier whilst conducting as well as relaxing [29].

The main advantage of using modulus spectroscopy is that, in this formalism the information about the electrode effect is suppressed and one can easily study the intrinsic effect of the sample that can originate from electro-active region (i.e., grain) in the sample. This formalism is also helpful in the study of conductivity relaxation time.

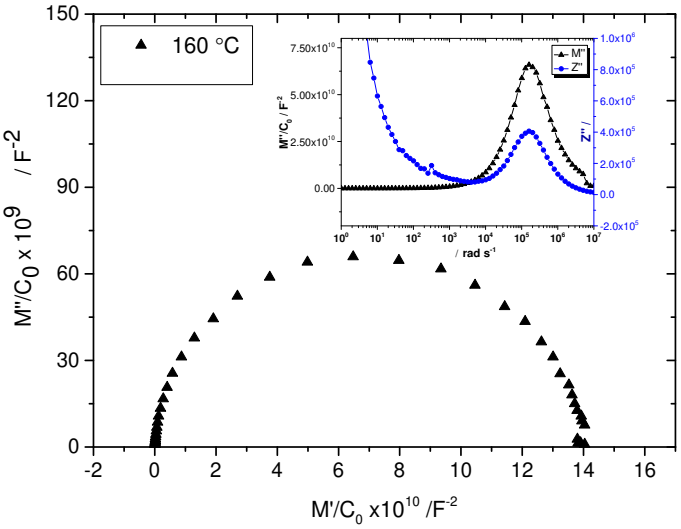

Fig. 10 Cole-Cole plot of M'/C_0 against M''/C_0 to exclude electrode effects. The inset is the frequency dependence of Z" and M''/C_0 at 160 °C.

Figure 10 is a plot manifesting the suppression of electrode effects when M'/C_0 is plotted against M''/C_0. A perfect semi circle is obtained. The inset shows how electrode effects seen in the low frequency tail of Z'' are supressed in the modulus formalism plot. In the inset it can be observed that Z'' and M'' peaks occur at the same frequency implying grain contribution to impedance relaxation.

3.3.4 Scaling.

Scaling is a vital feature in any data evaluation programn to normalize data for better comparison of different datasets. The study of the conductivity spectra and relaxation of conducting samples at different temperatures leads to scaling laws, $\sigma(\omega)/\sigma_{DC} = \sigma'/\sigma_o = F(\omega/\omega_c)$ and $M''/M''_{max} = F(\omega/\omega_c)$ respectively, known as the time–temperature superposition principle (TTSP) where ω_c is an arbitrarily determined

characteristic frequency[30,36].
Here, $\omega_c = \omega_p$ and $M''_{max} = M''(\omega_p)$. This scaling which collapses all datasets into one common curve indicates that the process can be resolved into a common physical mechanism modified only by thermodynamics scales[36].

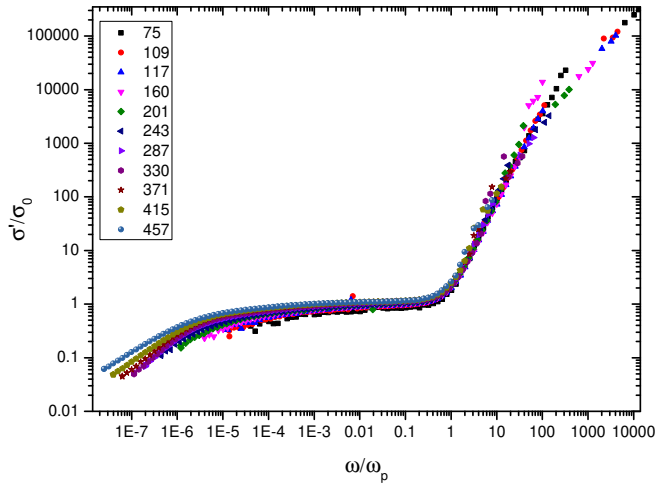

(a) Conductivity Scaling. The conductivity collapsed to a single curve indicating temperature independence of relaxation at higher frequency

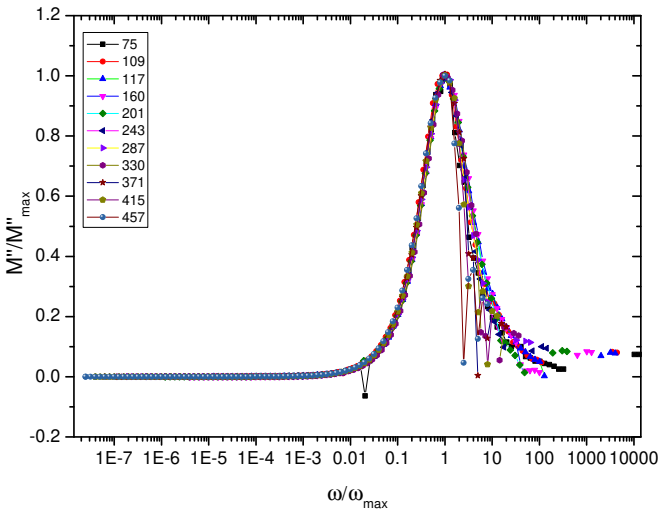

(b) Modulus Scaling. The modulus collapsed into a single curve and no electrode effect is observed at lower frequencies.

Fig. 11 Scaling formalism in conductivity and modulus.

Figure 11 shows the TTSP of conductivity and relaxation. In Figure 11a the conductivity spectra at different temperatures collapsed into a single curve at higher frequencies on appropriate scaling. However, the low frequency part of the plot does not collapse into a single plot due to varying contribution from electrode.

Furthermore, similar scaling of modulus as shown in Figure 11b reveals a perfect overlapping of different temperature data into a single master curve indicating a single relaxation process occuring within the sample. There is a perfect overlap even at low frequencies since modulus supresses electrode effects. This is also observed in the inset plot of Figure 10. From these findings, it is clear that the TTSP is observed implying that relaxation mechanism at the higher frequency is independent of temperature. Also observed in the Figure is the single boundary/knee at which crossover frequency occurs implying that the material has only single ionic species whose conductivity mechanism is independent of temperature.

Figure 12 shows the effect of thickness on the relaxation process as well as conductivity. It can be seen that all the plots for different thicknesses overlapped into single master plot both for conductivity and relaxation implying that the conduction mechanism (Figure 12) and relaxation (inset) are not dependent on thickness for films less than 32 μm investigated in this study.

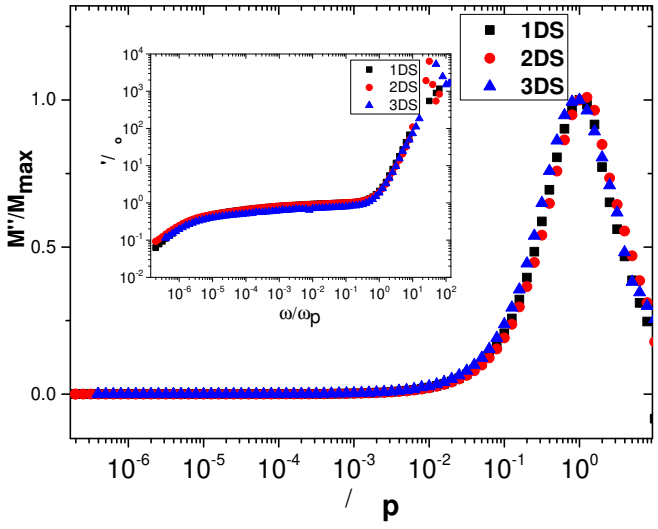

Fig. 12 Scaling vs Thickness

4 Conclusion

Electrical properties of NASICON thick films have been characterised. Spectral analysis have also been performed to study the ion dynamics. Thinner films densified well and consequently had higher surface conductivities than the thicker films, however at higher temperatures film thickness had no effect on ion conductivity. Spectral conductivity studies showed that Na^+ conduction was of long range hopping. Scaling studies showed that surface ion conductivity and relaxation were independent of temperature and thickness. Skin effect due to high frequency alternating electric-field also had no effect on surface conductivity because of the magnitudes of the conductivity values involved. Thick film

surface conductivity ($\sigma_{300^\circ C} = 1.26 \times 10^{-5}$ sq/Ω) is far less than bulk conductivity ($\sigma_{300^\circ C} = 2.51 \times 10^{-3}$ S/cm) reported in literature[37]. The values of conductivity and relaxation activation energies suggest that ions whilst conducting and relaxing overcome the same energy barrier. SEM investigation showed that there is a minimum thickness ($7\ \mu$m) for which NASICON can be printed and used in high temperature applications (up to 1100 °C) successfully and less than that, the entire film may undergo phase change, zirconia being the dominant secondary phase.

Acknowledgements

Funding from the Commonwealth Scholarship Council and the School of Chemical and Process Engineering is greatly appreciated.

References

1 H. Y. P. Hong, *Mater. Res. Bull.*, 1976, **11**, 173.
2 J. B. Goodenough, H. Y. P. Hong and J. A. Kafalas, *Mater. Res. Bull.*, 1976, **11**, 203.
3 N. Anantharamulu, K. K. Rao, G. Rambabu, B. V. Kumar and V. Radha, *J. Mater. Sci.*, 2011, **46**, 2821.
4 R. Stevens and J. P. G. Binner, *J. Mater. Sci*, 1984, **19**, 695.
5 G. M. Kale and K. T. Jacob, *J. Mater. Res.*, 1989, **4**, 417.
6 T. Zhong, B. Quan, X. Liang, F. Liu and B. Wang, *Mater. Sci. Eng. B*, 2008, **151**, 127 – 132.
7 G. M. Kale, A. J. Davison and D. J. Fray, *Solid State Ionics*, 1996, **86-88**, 1107.
8 K. Sahner, A. Schulz, J. Kita, R. Merkle, J. Maier and R. Moos, *Sensors*, 2008, **8**, 4774.
9 S. Yao, S. Hosohura, Y. Shimizu, N. Miura, H. Futata and N. Yamazoe, *Chem. Lett.*, 1990, 2069.
10 L. Wang and R. V. Kumar, *Solid State Ionics*, 2003, **158**, 309.
11 J. Alamo and R. Roy, *J. Am. Ceram. Soc.*, 1984, **67**, 78–80.
12 Y. Miyachi, G. Sakai, K. Shimanoe and N. Yamazoe, *Sensor. Actuat. B - Chem*, 2003, **93**, 250 – 256.
13 N. Izu, G. Hagen, D. Schonauer, U. Roder-Roith and R. Moos, *J.Ceram Soc. Japan*, 2011, **119**, 687–691.
14 N. B. Desai, K. Byrappa, A. B. Kulkarni and G. S. Gopalakrishna, *Bull. Mater. Sci*, 1987, **9**, 117–121.
15 K. Funke, *Prog. Solid State Chem.*, 1993, **22**, 111–195.
16 D. P. Almond., C. C. Hunter and A. R. West, *J. Mater. Sci.*, 1984, **19**, 3236–3248.
17 W. Bogusz, R. Sobiestuanskas, J. R. Dygas, F. Krok, A. Orliukas, E. Kozakievicius and A. Kezionis, *Molecul. Phys. Rep.*, 2000, **27**, 11–17.
18 G. Pasciak, W. Mielcarek, K. Prociow and J. Warycha, *Ceram. Int.*, 2014, **40**, 12783 – 12787.
19 S. Wiegartner, G. Hagen, J. Kita, R. Moos, M. Seufert, E. Glaser, K. Grimmel, A. Bolz, C. Schmaus and A. Kiessig, *IEEE Sensors Proc.*, 2001, 1014–1016.
20 J. C. Rautio and V. Demir, *IEEE Transactions on Microwave Theory and Techniques*, 2003, **51**, 915–921.
21 G. Collin and J. Boilot, *Superionic Solids and Solid Electrolytes*, Academic Press, 1989, pp. 227–263.
22 T. Kida, Y. Miyachi, K. Shimanoe and N. Yamazoe, *Sensor. Actuat. B.-Chem.*, 2001, **80**, 28 – 32.
23 F. Qiu, Q. Zhu, X. Yang, Y. Quan and L. Sun, *Sensor Actuat. B - Chem*, 2003, **93**, 237–242.
24 M. B. Heaney, in *The Measurement, Instrumentation and Sensors Handbook*, CRC Press, 1999, ch. Electrical Conductivity and Resistivity.
25 W. A. Maryniak, T. Uehara and M. A. Noras, *Surface Resistivity and Surface Resistance Measurements Using a Concentric Ring Probe Technique*, Trek Trek Application Note 1005, 2013.
26 R. O. Fuentes, F. M. B. Marques and J. I. Franco, *Bol. Soc. Esp. Ceram. V*, 1999, **38**, 631–634.
27 R. O. Fuentes, F. M. Figueiredo, F. M. B. Marques and J. I. Franco, *J. Eur. Ceram. Soc.*, 2001, **21**, 737 – 743.
28 A. K. Jonscher, *Nature*, 1977, **267**, 673–679.
29 C. R. Mariappan, G. Govindaraj and B. Roling, *Solid State Ionics*, 2005, **176**, 723–729.
30 G. Govindaraj and C. R. Mariappan, *Solid State Ionics*, 2002, **147**, 49 – 59.
31 T. Prakash, *Int. Nano Lett.*, 2012, **2**, 1–3.
32 C. R. Mariappan, G. Govindaraj, S. V. Rathan and G. V. Prakash, *Mater. Sci. Eng. B*, 2005, **121**, 2–8.
33 D. C. Sinclair, *Bol. Soc. Esp. Ceram. V*, 1995, **34**, 55–65.
34 H. E. Green, *IEEE Transactions on Microwave Theory and Techniques*, 1999, **47**, 365–366.
35 S. Basu and H. S. Maiti, *Ionics*, 2010, **16**, 111–115.
36 B. Roling, A. Happe, K. Funke and M. D. Ingram, *Phys. Rev. Lett.*, 1997, **78**, 2160–2163.
37 F. Lalere, J. B. Leriche, M. Courty, S. Boulineau, V. Viallet, C. Masquelier and V. Seznec, *J. Power Sources*, 2014, **247**, 975–980.